Journal of Power Sources 307 (2016) 220–230

Contents lists available at ScienceDirect

Journal of Power Sources

journal homepage: www.elsevier.com/locate/jpowsour

New method for parameter estimation of an electrochemical-thermal coupling model for $LiCoO_2$ battery

Junfu Li [a], Lixin Wang [a], Chao Lyu [a, *], Han Wang [b], Xuan Liu [a]

[a] School of Electrical Engineering and Automation, Harbin Institute of Technology, Harbin 150001, China
[b] School of Astronautics, Harbin Institute of Technology, Harbin 150001, China

HIGHLIGHTS

- A simplified electrochemical-thermal coupling model is proposed.
- Excitation response analysis is applied to obtain mechanistic parameters.
- Simulations agree with the measurements with satisfactory accuracy.

ARTICLE INFO

Article history:
Received 3 September 2015
Received in revised form
10 December 2015
Accepted 16 December 2015
Available online 8 January 2016

Keywords:
Accurate prediction of battery behaviors
Electrochemical-thermal coupling model
Excitation response analysis
Mechanistic parameters

ABSTRACT

An accurate prediction of battery behaviors guarantees the reliability, security, and efficiency for current tasks. An electrochemical-thermal (ECT) coupling model for $LiCoO_2$ battery is proposed to describe charge and discharge behaviors. With lumped thermal analysis, calculations of heat generation, conduction, and dissipation are added to a simplified electrochemical model. Battery mechanistic parameters are reasonably reduced and regrouped to reduce estimation complexity. Based on excitation response analysis, identification conditions are specially designed to obtain mechanistic parameters. Simulations are carried out to validate the applicability of model at different operating conditions. Simulation results of terminal voltage and surface temperature are in good agreement with actual experimental measurements at lower C rates and dynamic load currents. With proposed parameter estimation method, the simplified ECT coupling model can be applied to similar battery systems.

1. Introduction

Li-ion battery is popular for high-performance battery management system (BMS) because of its high working voltage, large energy density, low self-discharge rate, and no memory effect [1,2]. Equivalent circuit model (ECM) has been studied extensively for the purpose of vehicle power management control [1]. ECMs consist of a few electronic components (resistance, capacitance, and inductance) of which the parameters are obtained by impedance analysis or linear spline functions [3,4]. With simple formation and acceptable accuracy, ECM is commonly embedded in a microprocessor [5].

The pseudo 2 dimensional (P2D) model was based on theories of porous electrodes and concentrated solutions and was developed to capture the microcosmic behaviors of Li-ion at different operating conditions [6]. The development of the P2D model set the foundation for further research on mechanistic models [7–9]. The inputs of these models are mechanistic parameters, currents, and time. The P2D model can predict battery behaviors more accurately than ECMs [10]. The P2D model incorporates a description of the battery's internal thermal distribution, reliably simulating its internal and external behaviors [11–14]. Existing ECT models include coupled electrochemical and thermal components. Electrochemical processes affect the battery's internal thermal distribution, which in turn impacts the overpotentials and mechanistic parameters. Table 1, explicitly, compares different mechanistic models in terms of their applications.

As mechanistic models can accurately simulate the entire state of charge (SOC), they are very appealing in BMS [17,18]. However, the large computational cost of solving partial differential

* Corresponding author. P.O. Box 404, Harbin Institute of Technology, No. 92, West Dazhi Street, Nangang District, Harbin 150001, Heilongjiang, China.
E-mail addresses: 13B906023@hit.edu.cn (J. Li), wlx@hit.edu.cn (L. Wang), lu_chao@hit.edu.cn (C. Lyu), shirlycool88@163.com (H. Wang), liuxuan_hit@163.com (X. Liu).

http://dx.doi.org/10.1016/j.jpowsour.2015.12.058
0378-7753/

Table 1
Comparison on applications of different mechanistic models.

Author	Literature	Model	Positive material	Application
J. Vazquez-Arenas	[11]	P2D-thermal coupling	$LiNi_{1-x-y}Co_xMn_yO_2$	Parameter sensitivity analysis and external characteristic simulation
A. Tourani	[12]	P2D-thermal coupling	$LiFePO_4$, $LiMnO_2$	External characteristic simulation and thermal management
L.H. Saw	[13]	P2D-thermal coupling	$LiFePO_4$	Heat generation analysis and thermal management
K. Somasundaram	[14]	P2D-thermal coupling	$LiMnO_2$	Parameter design and thermal management
M. Doyle	[15]	P2D	$LiMnO_2$	Internal process and external characteristic simulation
E. Martinez-Rosas	[16]	P2D	$LiMnO_2$	Internal process and external characteristic simulation

equations limits the practical application of these models and thus many efforts have concentrated on simplifying these models [19–27]. On account of low computational cost, simplified models are more suitable for studies on mechanistic parameters [28]. Thus, it would be highly desirable to simplify these models, while preserving their essential physical characteristics [29].

Single particle (SP) is a simplified model that has been developed in Refs. [19–21]. With the assumption of uniform distribution over all particles inside electrodes, a single particle was used to represent each electrode and the distributions of physical properties were approximated by parabolic profiles. While the SP model can be quickly simulated, it is invalid at higher charge and discharge C rates [22]. Therefore, a description of concentration polarization overpotential was added to SP model to improve simulation precision [23–27]. Table 2 gives an explicit comparison of different simplified mechanistic models.

Generally, mechanistic models contain a number of parameters. The cell is dismantled into component electrodes and then most of these parameters are obtained by traditional electrochemical measurement methods [34–36]. For practical applications, a method of parameter estimation without battery destruction is needed. The most frequently used method for nondestructive parameter estimation is genetic algorithm (GA) [19,37,38]. The advantages of GA are: (i) the algorithm is flexible and can be optimized according to the selected objective function, (ii) the optimal solution of selected objective function can be found even when the initial parameters deviate from the optimal ones, (iii) the problem of algorithm convergence can be well solved in the case of the limited boundary condition. However, GA also has its limits: (i) the computing process of GA can sometimes last long due to the complicated battery model and objective function which needs to be calculated repeatedly, (ii) terminal condition is usually that the objective function reaches to the minimum as a whole. As to individual parameters, the identification results may fail to reflect the real situations. Moreover, the coupling relationships between the numerous parameters have an effect on identification results.

For further applications in BMS, the purpose of our work is to establish a simplified ECT coupling model with reduced and regrouped mechanistic parameters, which can simulate battery behaviors at different operating conditions. We propose a new method for nondestructive parameter estimation with a lower computational cost. Identification conditions are designed to obtain mechanistic parameters based on excitation response analysis. This paper is organized as follows: in Section 2, a simplified ECT coupling model is proposed; in Section 3, excitation response analysis is proposed, and the functional relationships between mechanistic parameters and external measurable variables are theoretically analyzed; in Section 4, necessary validations are presented.

2. ECT coupling model

2.1. Electrochemical model

Compared to a P2D model, the SP model has a simpler formation. However, the lack of description on liquid phase diffusion brings relatively large errors in simulation at higher C rates. In this section, we establish a simplified model with essential physics including liquid phase diffusion.

2.1.1. Basic working process

Based on the assumption that all of the particles in an electrode are represented by one particle and the current distribution is uniform over all of the particles, the pore wall flux of Li-ion is given as [10].

$$j_n^{cc} \approx IR_n/3F\left(1-\varepsilon_n-\varepsilon_{f,n}\right)l_nA \tag{1}$$

$$j_p^{cc} \approx -IR_p/3F\left(1-\varepsilon_p-\varepsilon_{f,p}\right)l_pA$$

The ratios between average and maximum Li-ion concentrations in the active material in the electrodes are defined as [10].

$$y_0=\frac{c_{p,0}^s}{c_{\max,p}^s},\quad x_0=\frac{c_{n,0}^s}{c_{\max,n}^s},\quad y_{avg}=\frac{c_{p,avg}^s}{c_{\max,p}^s},\quad x_{avg}=\frac{c_{n,avg}^s}{c_{\max,n}^s} \tag{2}$$

Where y_{avg} and x_{avg} are solid phase average stoichiometric numbers of electrodes. And y_0 and x_0 are initial values of y_{avg} and x_{avg}, respectively.

When the cell is charged or discharged, average Li-ion concentration in the electrodes at the current collectors is given as [10].

$$c_{i,avg}^s=c_{i,0}^s-\int_0^t 3\frac{j_i}{R_i}\mathrm{d}t\ ,\quad i=n,p \tag{3}$$

Applying Eqs.(1) and (2) in Eq. (3), the formulas of y_{avg} and x_{avg} are given as

Table 2
Comparison of different simplified mechanistic models on simplification.

Literature	Condition	Model	Simulation time	Simulation precision
[30]	Multi-rate constant-current discharge(<8C)	Reduced order P2D	1.5s	99%
[31]	Constant-current discharge	Finite-element orthogonal collocation P2D	2s	[a]
[32]	Multi-rate constant-current discharge	Reconfiguration P2D-thermal coupling	200ms	[a]
[33]	Multi-rate constant-current discharge(<5C)	Improved SP	2.1s	99%

[a] Not specified.

$$y_{avg} = y_0 + It/Q_p, x_{avg} = \left(1 - y_{ofs} - y_{avg}\right)Q_p/Q_n \tag{4}$$

Where Q_p and Q_n theoretically represent the maximum available capacities of effective active material in the electrodes and the definitions are given as

$$Q_i = c^s_{\max,i}F\left(1 - \varepsilon_i - \varepsilon_{f,i}\right)l_iA \ , \ i = n, p \tag{5}$$

We define y_{ofs} as the offset of relative position of stoichiometric numbers which can be given as

$$y_{ofs} = 1 - y_0 - x_0\frac{Q_n}{Q_p} \tag{6}$$

Basic working process can be described by the above four parameters (y_0, Q_p, Q_n, and y_{ofs}) and the process of parameter estimation will be discussed in detail in section 3.1.

2.1.2. Solid phase diffusion

Considering the solid phase diffusion effect, the average Li-ion concentration and volume-averaged concentration flux in the electrodes are given as [19,23,25,39].

$$\frac{\mathrm{d}}{\mathrm{d}t}c^s_{i,avg}(t) + 3\frac{j_i}{R_i} = 0 \ , \ i = n, p$$

$$\frac{\mathrm{d}}{\mathrm{d}t}q_{i,avg}(t) + 30\frac{D_{s,i}}{R_i^2}q_{i,avg}(t) + \frac{45}{2}\frac{j_i}{R_i^2} = 0 \tag{7}$$

$$35\frac{D_{s,i}}{R_i}\left(c^s_{i,surf}(t) - c^s_{i,avg}(t)\right) - 8D_{s,i}q_{i,avg}(t) = -j_i$$

Applying Eqs. (1)–(3) in Eq. (7), solid phase surface stoichiometric numbers of electrodes can be obtained

$$y_{surf}(t) = y_{avg}(t) + \Delta y'(t) \tag{8}$$

$$x_{surf}(t) = x_{avg}(t) - \Delta x'(t)$$

Where $\Delta y'$ and $\Delta x'$ are deviations between solid phase surface and average stoichiometric numbers of electrodes. The discrete formations of $\Delta y'$ and $\Delta x'$ can be found to be

$$\Delta y'(t_{k+1}) = \Delta y'(t_k) + \frac{1}{\tau_p^s}\left(\frac{12}{7}\frac{\tau_p^s}{Q_p}I(t_k) - \Delta y'(t_k)\right)(t_{k+1} - t_k) \tag{9}$$

$$\Delta x'(t_{k+1}) = \Delta x'(t_k) + \frac{1}{\tau_n^s}\left(\frac{12}{7}\frac{\tau_n^s}{Q_n}I(t_k) - \Delta x'(t_k)\right)(t_{k+1} - t_k)$$

Where τ_p^s and τ_n^s are solid phase diffusion time constants of electrodes and the definitions are given as [10].

$$\tau_i^s = \frac{R_i^2}{30D_{s,i}} \ , \ i = n, p \tag{10}$$

The solid phase surface stoichiometric numbers of electrodes directly determine the open circuit voltage (OCV). Therefore, OCV at the reference temperature is described as [10,40].

$$E^{ref}_{ocv}(t) = U_p\left(y_{surf}\right) - U_n\left(x_{surf}\right) \tag{11}$$

Where U_p and U_n are open circuit voltage curves of electrodes.

2.1.3. Liquid phase diffusion

The effect of liquid phase diffusion can be equivalently seen as the establishment of electrolyte concentration deviation at current collectors of each electrode. The degree of concentration polarization can be expressed by one fused state variable Δc^l [25].Therefore, we have

$$\eta_{con}(t) = \frac{2RT(t)}{F}(1 - t_+)\ln\left(\frac{c_0^l + \Delta c^l(t)}{c_0^l - \Delta c^l(t)}\right) \tag{12}$$

Where c_0^l is initial electrolyte concentration. We define Δc^l as the deviation of the electrolyte concentration between two current collectors

$$\Delta c^l(t) = P_{con}\left(1 - e^{-t/\tau_e}\right)I(t) \tag{13}$$

The discrete formation of Δc^l can be described as

$$\Delta c^l(t_{k+1}) = \Delta c^l(t_k) + \frac{1}{\tau_e}\left(P_{con}I(t_k) - \Delta c^l(t_k)\right)(t_{k+1} - t_k) \tag{14}$$

Where P_{con} and τ_e are the proportional coefficient of activation energy and time constant of liquid phase diffusion, respectively.

2.1.4. Reaction polarization

According to Butler-Volmer kinetics, reaction polarization overpotential η_{act} can be expressed as [10].

$$\eta_{\mathrm{act}} = \frac{2RT}{F}\left(\ln\left(\sqrt{m_n^2 + 1} + m_n\right) - \ln\left(\sqrt{m_p^2 + 1} + m_p\right)\right)$$
$$m_i = 0.5j_i \Big/ \left(k_i\left(c^s_{\max,i} - c^s_{i,surf}\right)^{0.5}\left(c^s_{i,surf}\right)^{0.5}\left(c_0^l\right)^{0.5}\right), \ i = n, p \tag{15}$$

Applying Eqs. (1)–(3) and (5) in Eq. (15), we have

$$\eta_{act}(t) = \frac{2RT(t)}{F}\left(\ln\left(\sqrt{m_n^2(t) + 1} + m_n(t)\right) + \ln\left(\sqrt{m_p^2(t) + 1} + m_p(t)\right)\right)$$
$$m_p(t) = \frac{1}{6Q_p{c_0^l}^{0.5}}\frac{1}{\left(1 - y_{surf}\right)^{0.5}\left(y_{surf}\right)^{0.5}}P_{act}I(t) \tag{16}$$
$$m_n(t) = \frac{1}{6Q_n{c_0^l}^{0.5}}\frac{1}{\left(1 - x_{surf}\right)^{0.5}\left(x_{surf}\right)^{0.5}}P_{act}I(t)$$

Where P_{act} is a lumped parameter and comparable to electrochemical reaction rate constant, which reflects the difficulty of electrochemical reaction.

2.1.5. Ohmic polarization

Additionally, the ohmic polarization overpotential η_{ohm} can be uniformly expressed as

$$\eta_{ohm}(t) = R_{ohm}I(t) \tag{17}$$

Where R_{ohm} is ohmic resistance expressed in the form of a lumped parameter.

Neglecting the thermal effect on OCV, terminal voltage U_{app} at reference temperature is found to be

$$U_{app}(t) = E_{ocv}^{ref}(t) - \eta_{con}(t) - \eta_{act}(t) - \eta_{ohm}(t) \tag{18}$$

2.2. Thermal model

The calculations of overpotentials in Eqs.(12) and (16) include the items of average internal temperature. Therefore, a volume average approach for the analysis of thermal behavior is employed in our work. It is assumed that spiral rolls battery with small capacity is an isothermal body. Thermal resistance model which is shown in Fig. 1 is adopted to describe heat conduction and dissipation in radial direction.

The heat generation rate $G(t)$ consists of two parts: irreversible heat generation rate $\dot{Q}_{ir}$ and reversible heat generation rate $\dot{Q}_r$ [41], which can be described as

$$\dot{Q}_{ir}(t) = I(t)(\eta_{con}(t) + \eta_{act}(t) + \eta_{ohm}(t)),$$
$$\dot{Q}_r(t) = -I(t)T(t)\frac{dE_{ocv}(t)}{dT} \tag{19}$$

$$G(t) = \dot{Q}_{ir}(t) + \dot{Q}_r(t) \tag{20}$$

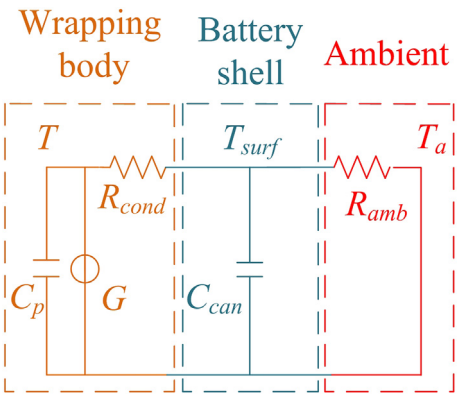

Fig. 1. Thermal resistance model in radial direction.

Where T is defined as internal average temperature and $dE_{ocv}(t)/dT$ is battery material inherent attribute which is a function of stoichiometric number of each electrode [2,42,43].

$$\frac{dE_{ocv}(t)}{dT} = \left.\frac{dE_{ocv}(t)}{dT}\right|_p - \left.\frac{dE_{ocv}(t)}{dT}\right|_n \tag{21}$$

Heat dissipation rate $G_{exchange}$ can be given as

$$G_{exchange}(t) = \left(T_{surf}(t) - T_a(t)\right)\Big/R_{amb} \tag{22}$$

$$R_{amb} = 1/hA_0$$

Where h, A_0, T_a, and T_{surf} are heat transfer coefficient, effective heat dissipation area, ambient temperature, and surface temperature, respectively. The positive value of $G_{exchange}$ indicates that the cell dissipates heat to the environment.

According to the thermal resistance model and energy flow, T and $Tsurf$ can be given as

$$m_{roll}C_p\frac{dT(t)}{dt} = G(t) - \frac{T(t) - T_{surf}(t)}{R_{cond}} \tag{23}$$

$$m_{can}C_{can}\frac{dT_{surf}(t)}{dt} = \frac{T(t) - T_{surf}(t)}{R_{cond}} - G_{exchange}(t) \tag{24}$$

Where m_{roll} and m_{can} are mass of wrapping body of electrode and battery shell. C_p and C_{can} are heat capacity ratios of wrapping body of electrode and battery shell, respectively. R_{cond} is thermal resistance. In order to calculate T, Eq. (23) is given in discrete formation

$$T(t_k) = T(t_{k-1}) + (t_k - t_{k-1})\left(G(t_{k-1}) - \left(T(t_{k-1}) - T_{surf}(t_{k-1})\right)\Big/R_{cond}\right)\Big/(m_{roll}C_p) \tag{25}$$

At current internal temperature T and reference temperature T_{ref}, battery OCV in Eq. (18) is then modified by Nernst equation [2].

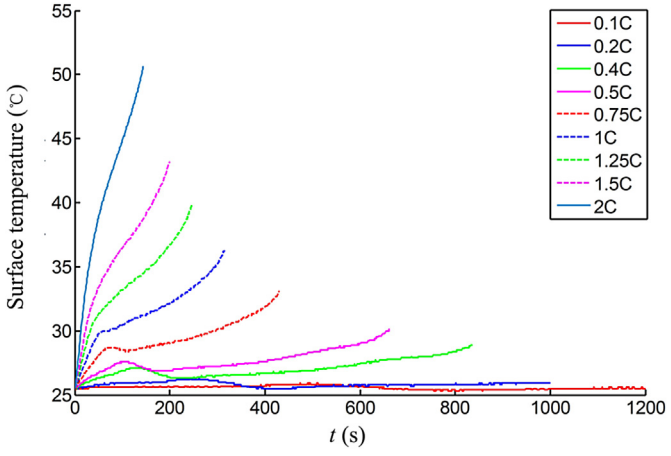

Fig. 2. Variations of surface temperature at different discharge C rates and 25 °C ambient temperature.

Table 3
Values of inherent characteristic parameters [12–14,25].

Parameters	Values
A_0 (m^2)	0.0037
C_{can} (J kg^{-1} K^{-1})	460
C_p (J kg^{-1} K^{-1})	1000
c_0^l(mol m^{-3})	1000
F (C mol^{-1})	96485.3
m_{can} (kg)	0.0013
m_{roll} (kg)	0.040
R (J mol^{-1} K^{-1})	8.314
t_+ (−)	0.363
T_{ref} (K)	298.15

$$E_{ocv}(t) = E_{ocv}^{ref}(t) + \left(T(t) - T_{ref}\right)\frac{dE_{ocv}(t)}{dT} \tag{26}$$

It should be emphasized that the values of some mechanistic parameters are related to temperature and the functional relationships between them will be discussed in detail in the following section.

3. Excitation response analysis

Variations of surface temperature at different discharge C rates and 25 °C ambient temperature are shown in Fig. 2. It is observed that surface temperature rising with respect to time is not phenomenal at lower C rates, and the amplitude of surface temperature variation is relatively small at larger C rates over a short period of time. Consequently, we speculate that battery internal temperature is approximately equal to the surface temperature during this period, which contributes to decouple the interaction effects of complicated physicochemical processes.

The parameters of the proposed model can be classified into two categories: inherent characteristic parameters and mechanistic parameters. Inherent characteristic parameters (e.g., c_0^l and A_0) which are listed in Table 3 can be obtained by consulting manufacturers directly or measuring. In this section, we will make a detailed analysis on the physics of the proposed model and establish the analytical functional relationships bewteen mechanistic parameters and measurable variables sequentially.

3.1. Parameter estimation of basic working process

According to the definitions in section 2.1.1, another kind of calculation formula of Q_p and Q_n is described as

$$Q_p = \frac{Q_{all}}{Dy}, Q_n = \frac{Q_{all}}{Dx} \tag{27}$$

Where Q_{all} is total capacity tested at discharge rate of 0.02C. D_x and D_y are maximum variation ranges of stoichiometric number x and y, respectively. The two kinds of expression forms of Q_p and Q_n have the same physical meanings. Using standard Coulomb counting, SOC of the battery can be defined as [1,4].

$$soc(t) = 1 - \frac{It}{Q_{all}} \tag{28}$$

Neglecting the effects of diffusion process inside the battery, ideal OCV tested at small discharge C rate can be obtained by merging Eqs. (4), (6), (27) and (28)

$$E_{ocv}^{ref}(t) = U_p\left(y_0 + D_y(1 - soc(t))\right) - U_n(x_0 + D_x(1 - soc(t))) \tag{29}$$

Measured voltage can be regarded as $E_{ocv}^{ref}(t)$. Terminal voltage and surface temperature profiles are shown in Fig. 3. Surface temperature fluctuates on a tiny scale and is proximate to the controlled ambient temperature. With the previous speculation, the effect of internal temperature on $E_{ocv}^{ref}(t)$ can be ignored. Least square fit is adopted to fit for initial stoichiometric numbers (x_0 and y_0) and their variation ranges (D_x and D_y). The fitting input variables are the sequences of terminal voltages and *soc* calculated by load current and time. Then, Q_p, Q_n, and y_{ofs} can be obtained by Eqs.(27) and (6).

3.2. Estimation of ohmic resistance

Compared to mass transfer processes, electrical conductive speed generated by ohmic polarization is much faster. And ohmic resistance can be calculated by current response stimulated by a low sine voltage input with 1 kHz frequency.

Temperature has an influence on ohmic resistance which is measured at different ambient temperatures after the rest time of 1 h. Internal temperature is similar to the ambient temperature at no load currents. The variations of ohmic resistance with respect to temperature are fitted by the following Arrhenius formula [2].

$$R_{ohm} = R_{ohm}^{ref}\exp\left(\lambda_{ohm}\left(1/T_{ref} - 1/T\right)\right) \tag{30}$$

Where R_{ohm}^{ref} and λ_{ohm} are fitting parameters. The fitting input

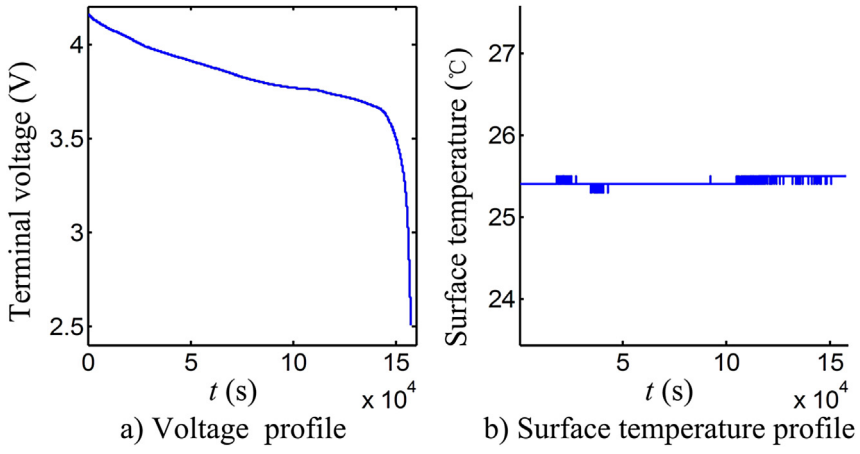

Fig. 3. Voltage and surface temperature profiles measured at discharge C rate of 0.02C and 25 °C ambient temperature.

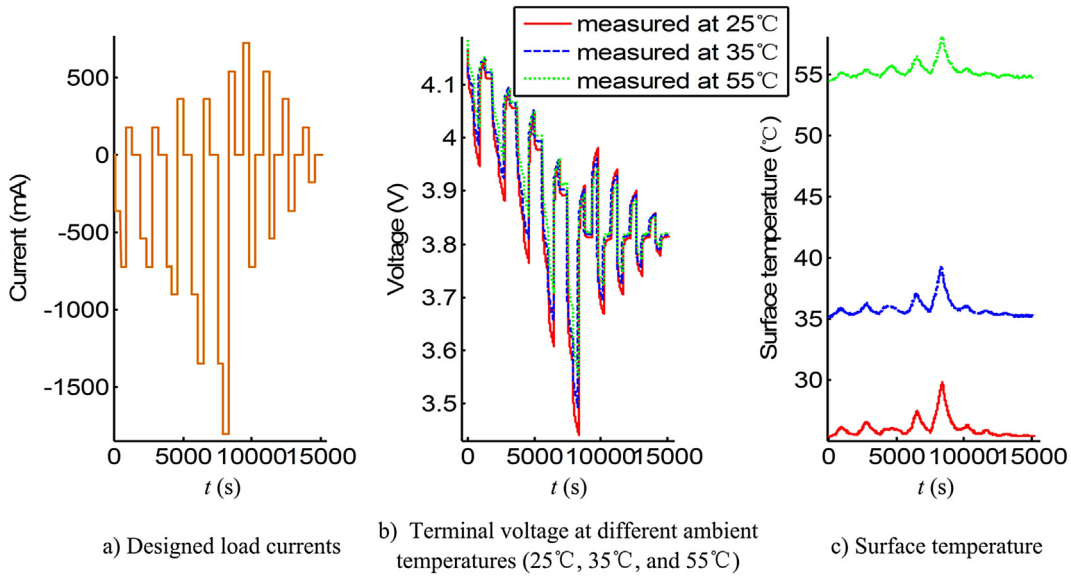

Fig. 4. Profiles of designed load currents, terminal voltage, and surface temperature at different ambient temperatures (25 °C, 35 °C, and 55 °C).

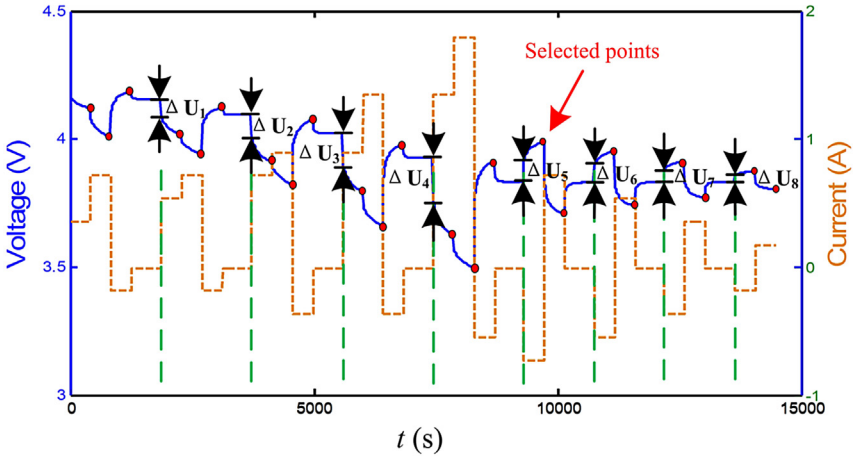

Fig. 5. The schematic diagram of selected measurable variables based on excitation response analysis. Δ*U* occurs when load current changes from zero to the certain value. Steady concentration deviations have been built at the selected points.

variables are R_{ohm} measured at four ambient temperatures (15 °C, 25 °C, 35 °C, and 55 °C).

3.3. Reaction polarization calculation

Dynamic operating condition is specially designed based on the response time of different physicochemical processes. Profiles of designed load currents, terminal voltage, and surface temperature at different ambient temperatures (25 °C, 35 °C, and 55 °C) are shown in Fig. 4. Measurement accuracy of ±0.1 °C accounts for the unsmooth profile of surface temperature.

As is shown in Fig. 5, when load current changes from zero to the certain value, ΔU which consists of η_{act} and η_{ohm} occurs. With obtained R_{ohm}^{ref} and λ_{ohm} in section 3.2, η_{act} can be indirectly calculated. P_{act} changes with the temperatures and Arrhenius formula is also employed to modify the parameter as

$$P_{act} = P_{act}^{ref} \exp\left(\lambda_{act}\left(1/T_{ref} - 1/T\right)\right) \tag{31}$$

According to Eq. (16), fitting parameters P_{act}^{ref} and λ_{act} can be acquired through least square fit. The fitting input variables are the sequences of η_{act}, I, and solid phase average stoichiometric numbers calculated by Eq. (4).

3.4. Estimation of parameters related to diffusion processes

When step current is applied to the battery, Li-ion concentration in the electrodes will not mutate immediately. Steady concentration deviations will be established between solid phase average and surface stoichiometric numbers after a period of transition time. Similarly, electrolyte concentration deviation between two current collectors of electrodes needs certain transition time to be stable. Thus, stable deviations can be given by Eqs.(9) and (14)

$$\Delta y'_{stable}(t) = 2\frac{\tau_p^s}{Q_p} I(t), \Delta x'_{stable}(t) = 2\frac{\tau_n^s}{Q_n} I(t), \Delta c_{stable}^l(t) = P_{con} I(t) \tag{32}$$

As is shown in Fig. 5, steady concentration deviations have been

built at the selected points. And terminal voltage can be described as

$$U_{app}(t) = \left(U_p\left(y_{avg} + \Delta y'_{stable}\right) - U_n\left(x_{avg} - \Delta x'_{stable}\right)\right) - \eta_{con}^{stable}(t) - \eta_{act}(t) - \eta_{ohm}(t) \tag{33}$$

The sequence of $U_{app}(t)$ in Eq. (33) is directly measured and after transformation, we have

$$U(t) = \left(U_p\left(y_{avg}(t) + \Delta y'_{stable}(t)\right) - U_n\left(x_{avg}(t) - \Delta x'_{stable}(t)\right)\right) - 2\frac{RT(t)}{F}(1-t_+)\ln\left(\frac{c_0 + \Delta c^l_{stable}(t)}{c_0 - \Delta c^l_{stable}(t)}\right) \tag{34}$$

Least square fit is employed to obtain τ_p^s, τ_n^s, and P_{con} simultaneously. The sequence of $U(t)$ on the left side of Eq. (34) is a merged fitting input variable, including three known sub parts: $U_{app}(t)$, $\eta_{act}(t)$ and $\eta_{ohm}(t)$. P_{con} with respect to temperature is fitted by

$$P_{con} = P_{con}^{ref}\exp\left(\lambda_{con}\left(1/T_{ref} - 1/T\right)\right) \tag{35}$$

Where P_{con}^{ref} and λ_{con} are fitting parameters. The fitting input variable is previously estimated P_{con}. And the value of T in Eq. (35) is replaced with ambient temperature.

Transforming Eq. (18), η_{con} is given as

$$\eta_{con}(t) = E_{ocv}^{ref}(t) - U_{app}(t) - \eta_{act}(t) - \eta_{ohm}(t) \tag{36}$$

Then, η_{con} can be obtained based on previous estimation results. Transforming Eq. (12), $\Delta c^l(t)$ is given as

$$\Delta c^l(t) = c_0^l\frac{\exp(\eta_{con}(t)F/(2RT(t)(1-t_+))) - 1}{\exp(\eta_{con}(t)F/(2RT(t)(1-t_+))) + 1} \tag{37}$$

The discrete formation of τ_e is found to be

$$\tau_e(t_{k+1}) = \frac{P_{con}\cdot I(t_k) - \Delta c^l(t_k)}{\Delta c^l(t_{k+1}) - \Delta c^l(t_k)}\cdot(t_{k+1} - t_k) \tag{38}$$

The average value of τ_e is then taken as the final result.

3.5. Thermal calculation

3.5.1. Estimation of heat transfer coefficient h

As h is only correlated to the ambient, it can be obtained independently. When load current is zero, heat generation accordingly turns into zero. Then Eq. (24) is found to be

$$-hA_0\left(T_{surf}(t) - T_a(t)\right) = m_{can}C_{can}\frac{dT(t)}{dt} \tag{39}$$

With the previous speculation, we have $T_{surf}(0) = T_0$ and $T_{surf}(\infty) = T_a$. Therefore, analytical solution of Eq. (39) can be given as

$$T_{surf}(t) = T_a + (T_0 - T_a)\exp(-hA_0t/(C_pm_{roll})) \tag{40}$$

$$\tau_{heat} = C_pm_{roll}/(hA_0)$$

Where τ_{heat} is time constant of heat dissipation. The cell is tested in the thermal chamber and temperature sensor is tightly placed on the surface of the battery. Surface temperature variations are related to different operating scenarios. After being discharged at different discharge C rates, battery surface temperature restores to ambient temperature gradually. τ_{heat} is then obtained by fitting Eq. (40). The fitting input variable is the sequence of T_{surf}. According to the fitting result, h can be calculated.

3.5.2. Estimation of heat resistance R_{cond}

3.5.2.1. Overpotentials are related to internal temperature. If they are overestimated or underestimated, thermal calculation will bring larger errors. Therefore, $\dot{Q}_{ir}$ is replaced with

$$\dot{Q}_{ir} = I(t)(E_{ocv}(t) - U_{app}(t)) \tag{41}$$

Combining Eqs. (20), (21) and (41), $G(t)$ is obtained as

$$G(t) = I(t)\left(E_{ocv}^{ref}(t) - U_{app}(t) - T_{ref}\left(\left.\frac{dE_{ocv}(t)}{dT}\right|_p - \left.\frac{dE_{ocv}(t)}{dT}\right|_n\right)\right) \tag{42}$$

The previously designed dynamic operating condition is also used in this section. In order to calculate T_{surf}, Eq. (24) is given in discrete formation

$$T_{surf}(t_k) = \frac{\left(T_{surf}(t_{k-1})m_{can}C_{can}R_{cond} + (t_k - t_{k-1})(T(t_k) + R_{cond}A_0hT)_a\right)}{m_{can}C_{can}R_{cond} + (t_k - t_{k-1}) + R_{cond}(t_k - t_{k-1})A_0h} \tag{43}$$

Combining Eqs. (25) and (43), the unique value of R_{cond} can be obtained.

To describe the proposed model in an organized way, the primary parts of the proposed ECT coupling model are listed in Table 4, mentioning what portion is based on empirical behaviors and what portion relies on the physics. Validations for parameter estimation and proposed model will be discussed in the following section.

4. Validations and discussions

4.1. Validation for parameter estimation

Cylindrical batteries manufactured by Tianjin Lishen Battery Joint-Stock Co.(Tianjin, China), labeled LS.LR1865BC were used in the experiments. The battery specifications are summarized in Table 5. Experimental terminal voltage data were acquired by battery testing system (Neware BTS-5V-6A, China) using 1-s interval and the experimental surface temperature data were acquired by auxiliary equipment (Neware BTS-AUX, China) with a temperature sensor.

The procedure of mechanistic parameter identification is shown as follow:

Step a. A small discharge rate of 0.02C is applied to the battery at temperature of 25 °C in incubator to obtain four parameters (x_0, y_0, D_x, and D_y) of basic operating process through least square fit. Then,

Table 4
The primary parts of simplified ECT coupling model.

	Simplified ECT coupling model	Mechanistic parameters
Physics		
Terminal voltage	$U_{app}(t) = E_{ocv}(t) - \eta_{con}(t) - \eta_{act}(t) - \eta_{ohm}(t)$	
Nernst equation	$E_{ocv}(t) = E_{ocv}^{ref}(t) + (T(t) - T_{ref})\frac{dE_{ocv}(t)}{dT}$	
Basic working process	$E_{ocv}^{ref}(t) = U_p(y_{surf}) - U_n(x_{surf})$	
	$y_{avg} = y_0 + It/Q_p$	y_0 Q_p
	$x_{avg} = (1 - y_{ofs} - y_{avg})Q_p/Q_n$	y_{ofs} Q_n
Solid phase diffusion	$y_{surf}(t) = y_{avg}(t) + \Delta y'(t)$	
	$x_{surf}(t) = x_{avg}(t) - \Delta x'(t)$	
	$\Delta y'(t_{k+1}) = \Delta y'(t_k) + \frac{1}{\tau_p^s}(\frac{12}{7}\frac{\tau_p^s}{Q_p}I(t_k) - \Delta y'(t_k))(t_{k+1} - t_k)$	τ_p^s
	$\Delta x'(t_{k+1}) = \Delta x'(t_k) + \frac{1}{\tau_n^s}(\frac{12}{7}\frac{\tau_n^s}{Q_n}I(t_k) - \Delta x'(t_k))(t_{k+1} - t_k)$	τ_n^s
Liquid phase diffusion	$\eta_{con}(t) = \frac{2RT(t)}{F}(1 - t_+)\ln\left(\frac{c_0^l + \Delta c^l(t)}{c_0^l - \Delta c^l(t)}\right)$	
	$\Delta c^l(t_{k+1}) = \Delta c^l(t_k) + \frac{1}{\tau_e}(P_{con}I(t_k) - \Delta c^l(t_k))(t_{k+1} - t_k)$	τ_e
Reaction polarization	$\eta_{act}(t) = \frac{2RT(t)}{F}(\ln(\sqrt{m_n^2(t) + 1} + m_n(t)) + \ln(\sqrt{m_p^2(t) + 1} + m_p(t)))$	
	$m_p(t) = \frac{1}{6Q_p c_0^{l\,0.5}}\frac{1}{(1 - y_{surf})^{0.5}(y_{surf})^{0.5}}P_{act}I(t)$	
	$m_n(t) = \frac{1}{6Q_n c_0^{l\,0.5}}\frac{1}{(1 - x_{surf})^{0.5}(x_{surf})^{0.5}}P_{act}I(t)$	
Ohmic polarization	$\eta_{ohm}(t) = R_{ohm}I(t)$	
Heat generation	$G(t) = I(t)\left(\eta_{con}(t) + \eta_{act}(t) + \eta_{ohm}(t) - T(t)\frac{dE_{ocv}(t)}{dT}\right)$	
Thermal calculation	$T(t_k) = T(t_{k-1}) + (t_k - t_{k-1})\left(G(t_{k-1}) - \frac{(T(t_{k-1}) - T_{surf}(t_{k-1}))}{R_{cond}}\right)\frac{1}{m_{roll}C_p}$	R_{cond}
	$T_{surf}(t_k) = \frac{(T_{surf}(t_{k-1})m_{can}C_{can}R_{cond} + (t_k - t_{k-1})(T(t_k) + R_{cond}A_0hT_a))}{m_{can}C_{can}R_{cond} + (t_k - t_{k-1}) + R_{cond}(t_k - t_{k-1})A_0h}$	h
Empirical behaviors		
	$R_{ohm} = R_{ohm}^{ref}\exp(\lambda_{ohm}(1/T_{ref} - 1/T))$	$R_{ohm}^{ref}\lambda_{ohm}$
	$P_{act} = P_{act}^{ref}\exp(\lambda_{act}(1/T_{ref} - 1/T))$	$P_{act}^{ref}\lambda_{act}$
	$P_{con} = P_{con}^{ref}\exp(\lambda_{con}(1/T_{ref} - 1/T))$	$P_{con}^{ref}\lambda_{con}$

y_{ofs}, Q_p, and Q_n can be obtained by Eqs. (6) and (27); Step b. R_{ohm} is measured by battery resistance testing equipment after rest time of 40 min at different ambient temperatures, and its functional relationship with respect to temperature is obtained through least square fit;

Step c. Dynamic operating condition is especially designed according to Section 3.3 and 3.4. We extract the sequence of ΔU when load current suddenly changes. As the law of variation of R_{ohm} with respect to internal temperature is obtained at Step b, the sequence of η_{act} can be indirectly calculated. Lumped parameters P_{act}^{ref} and λ_{act} are obtained through least square fit;

Step d. The method of least square fit is also employed to obtain τ_p^s, τ_n^s, and P_{con} simultaneously by Eq. (34). As τ_p^s and τ_n^s are similar at different temperatures, the average of each parameter is selected as the final value. P_{con} with respect to temperature is fitted by Arrhenius formula. On the basis of previous mechanistic parameter estimation, each item on the right side of Eq. (36) can be obtained. Furthermore, τ_e can be calculated by Eq. (38) and the average value of τ_e is taken as the final result.

Step e. After being discharged at different discharge C rates, surface temperature restores to ambient temperature gradually. τ_{heat} is then obtained by fitting Eq. (40) and according to the fitting result, h then can be calculated;

Step f. With the previously designed dynamic operating condition, R_{cond} is obtained according to Section 3.5.2. As it does not vary much at different ambient temperatures, the average of R_{cond} is taken as the final value.

Parameter identification conditions are shown in Figs. 2–5 and the flowchart of parameter estimation is shown in Fig. 6. Results of least square fit and all estimated mechanistic parameters are listed in Tables 6 and 7, respectively. Statistical results show that root mean square error in each step is small which indicates that the proposed method for parameter estimation is valid.

Table 5
Battery specifications.

Specifications	Value
Pack Dimension t	Height: 65.0 ± 0.3 mm Width: 18.0 ± 0.2 mm
Weight	Approx: 40 g
Rated capacity	1800 mAh
Reference voltage	3.7 V
Cut-off voltage of charging	4.2 V
Positive material	$LiCoO_2$
Negative material	Graphite

4.2. Validation for charge and discharge behaviors

An accurate ECT coupling model can be applied to various operating conditions. Measurements and simulations at different C rates corresponding to two ambient temperatures are compared in Fig. 7.

The scopes of average absolute error (AAE) of terminal voltage and surface temperature are 35.58–194.84 mV (at 25 °C), 32.70–156.46 mV (at 40 °C) and 0.22–1.05 °C (at 25 °C), 0.18–1.64 °C (at 40 °C), respectively. When C rate is less than 1, the AAEs of terminal voltage and surface temperature are less than 70 mV and 1 °C, respectively, increasing along with the increment of C rate. And when C rate is more than 1, the AAE of terminal voltage will increase by 40–60 mV along with 0.5C increment of C rate. The AAEs of terminal voltage are relatively lower at 40 °C ambient temperature. The essence of such phenomenon is that ohmic and reaction polarization overpotentials are smaller at higher ambient temperatures, and the influence of polarization overpotentials on terminal voltage is relatively minor.

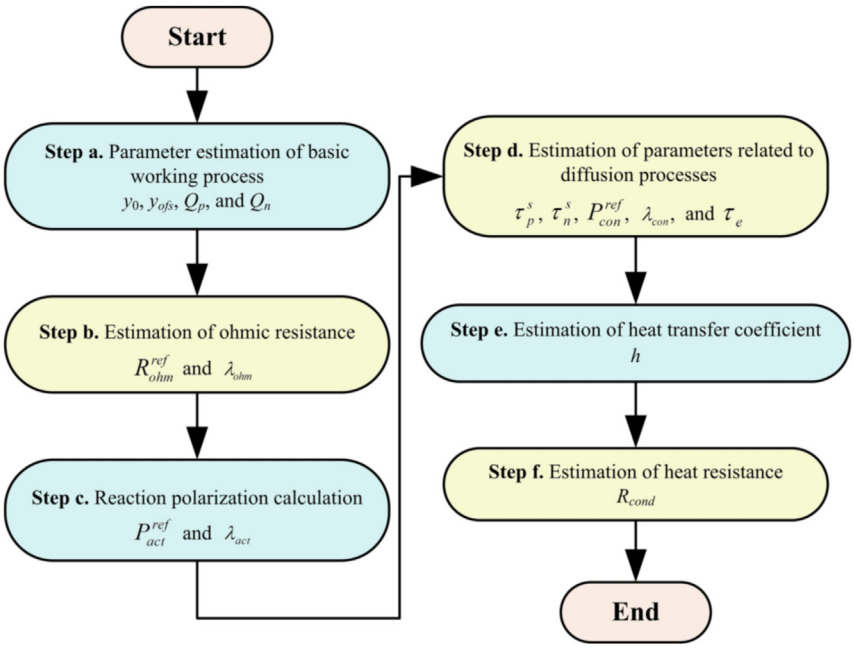

Fig. 6. Flowchart of parameter estimation.

Table 6
Results of least square fit.

Fitting parameters	Fitting variable	Root mean	Square error
Step a	y_0, x_0, D_y, and D_x	E_{ocv}^{ref}	0.0084(V)
Step b	R_{ohm}^{ref} and λ_{ohm}	R_{ohm}^{ref}	0.0011(Ω)
Step c	P_{act}^{ref} andλ_{act}	η_{act}	0.0096(V)
Step d	$\tau_p^s\tau_n^s$, andP_{con}	$U(t)$	0.0190(V)
	P_{con}^{ref} andλ_{con}	P_{con}	21.21(mol m^{-3} A^{-1})
Step e	τ_{heat}	T_{surf}	0.082(K)

The scopes of maximum absolute error (MAE) of terminal voltage and surface temperature are 76.25–343.11 mV (at 25 °C), 60.32–700.86 mV (at 40 °C) and 0.54–1.61 °C (at 25 °C), 0.73–2.97 °C (at 40 °C), respectively. It is seen from Fig. 7 that the simulation results agree with the experimental data at lower discharge C rates (0.2C/0.36A, 0.5C/0.9A and 1.0C/1.8A) and charge C rate (0.5C/0.9A). The errors are relatively large at high discharge C rates (1.5C/2.7A and 2.0C/3.6A) and charge C rate (1.0C/1.8A). We speculate that the reasons are: (1) The simulation accuracy at higher C rates may be limited by the formulation of liquid phase diffusion. If C rate is larger, the previous assumption on uniform distribution over all of the particles may be invalid, (2) The simulation errors of Q_{ir} and $G(t)$ determined by polarization overpotentials in Eqs.(19) and (25) are larger at higher C rates, which also affects the simulation accuracy of surface temperature by Eq. (43). Besides, the estimated numerical values of τ_p^s and τ_n^s may be larger and consequently, y_{surf} and x_{surf} are relatively larger by Eq. (8) which affects the terminal voltage profile approaching to the end of discharge. Thus, the discharge cut-off voltages are predicted in advance at lower discharge C rates.

Table 7
Values of estimated mechanistic parameters.

Parameter	Value	Parameter	Value
y_0 (−)	0.4493	τ_p^s(s)	106.0094
y_{ofs} (−)	0.1271	τ_n^s(s)	28.0436
Q_p (A s)	1.3636×10^4	P_{con}^{ref}(mol m^{-3} A^{-1})	607.1404
Q_n (A s)	8.4005×10^3	λ_{con}(K)	−695.4776
R_{ohm}^{ref}(Ω)	0.0761	τ_e(s)	67.7854
λ_{ohm}(K)	−342.7862	h (W m^{-2} K^{-1})	17.2446
P_{act}^{ref}(m$^{-1.5}$ mol$^{0.5}$ s)	6.0025×10^5	R_{cond} (K W^{-1})	1.1125
λ_{act}(K)	-5.7224×10^3		

Comparative results of measurements and simulations at dynamic load currents corresponding to two ambient temperatures are shown in Fig. 8. MAEs of terminal voltage and surface temperature are 56.70 mV (at 20 °C), 49.75 mV (at 45 °C) and 0.79 °C (at 20 °C), 0.52 °C (at 45 °C), respectively. As is seen in Fig. 8, when the battery is rested or charged, terminal voltage increases accordingly. Unlike the profile at the constant-current conditions, surface temperature varies over a small scale of 1 °C. We speculate that the reason may be: when the battery is charged or discharged during a period of time at the constant-current conditions, the sign of $G(t)$ basically does not alter, and surface temperature will increase. However, as the sign of dynamic load current changes at intervals, the numerical value of $G(t)$ will be affected by Eqs. (19) and (20). Especially, if the load current is zero, $G(t)$ will convert to zero, and the battery internal temperature T and surface temperature T_{surf} will decrease the amount as indicated by Eqs. (25) and (43), which qualitatively explains why the temperature varies over a small scale only.

5. Conclusions

This paper introduces a simplified ECT coupling model with essential physics. The original mechanistic parameters are reasonably reduced and regrouped. Parameter identification conditions are specially designed based on excitation response analysis. Simulations are carried out to validate the applicability of model at different load currents. The estimated terminal voltage and surface temperature accurately agree with the experiments at lower C rates and dynamic load currents. Due to the model formation of liquid phase diffusion and the assumption on uniform distribution over all of the particles, the errors are relatively large at higher C rates compared to the other mechanistic models [30–33].

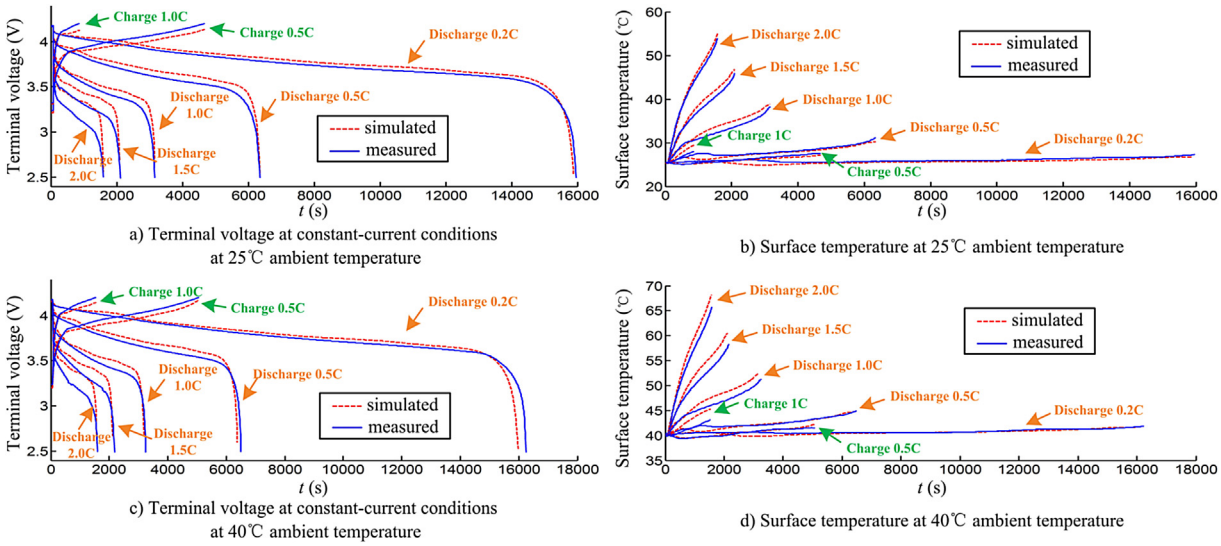

Fig. 7. Comparative results of measurements and simulations at different C rates corresponding to two ambient temperatures (25 °C and 40 °C).

Thus future work should focus on further model modification to achieve higher accuracy.

The contributions of the current study are summarized as below: (1) A simplified ECT coupling model is proposed with reduced or regrouped mechanistic parameters. (2) A new method for parameter estimation is creatively presented. The proposed model can simulate battery behaviors at different operating conditions. And mechanistic parameters of individual cell can be obtained through proposed method which has a lower computational cost compared to other methods [2,19,36–38]. In addition, the simplified ECT coupling model can also be applied to similar types of battery system, e.g., $LiNi_{1-x-y}Co_xMn_yO_2$, $LiFePO_4$, and vanadium batteries. The potential application of our work is that it can be applied to estimate SOC of single cell with the functional relationship between SOC and stoichiometric numbers. The model mechanistic parameters can also be used as features to assess battery health state. The remaining useful life of battery can be predicted by analyzing the variations of parameters at different aging stages. Moreover, online equalization based on this work could potentially improve the cycle life of battery stacks.

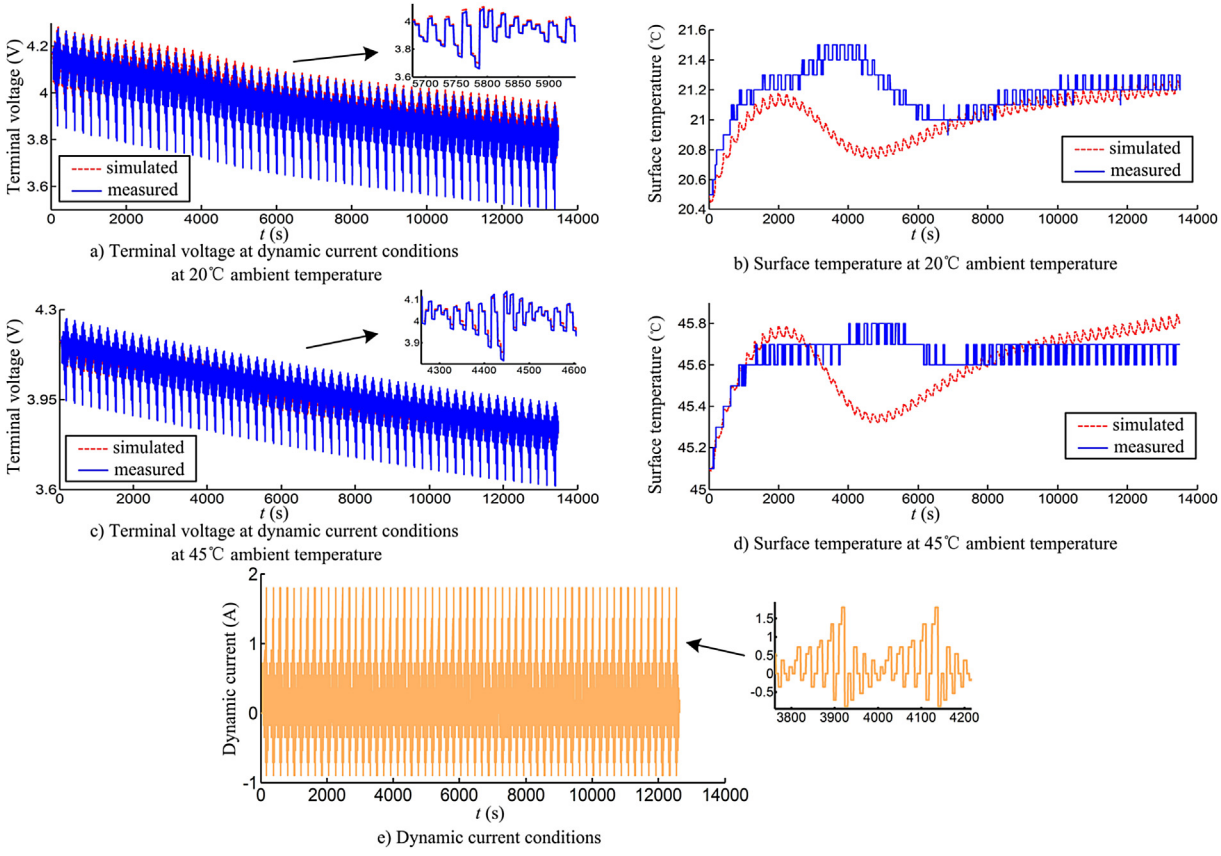

Fig. 8. Comparative results of measurements and simulations at dynamic load currents corresponding to two ambient temperatures (20 °C and 45 °C).

Acknowledgment

We thank the National Natural Science Foundation of China (No. 51477037) for financial support. We sincerely appreciate the significant help on translation supported by Miss. Jia Xie.

References

[1] H. Xiaosong, L. Shengbo, P. Huei, J. Power Sources 198 (2012) 359–367.
[2] L. Zhang, L. Wang, G. Hinds, C. Lyu, J. Zheng, J. Li, J. Power Sources 270 (2014) 367–378.
[3] M. Dubarry, B.Y. Liaw, J. Power Sources 174 (2007) 856–860.
[4] Y. Hu, S. Yurkovich, Y. Guezennec, B.J. Yurkovich, J. Power Sources 196 (2011) 449–457.
[5] X. Hu, F. Sun, Y. Zou, Simul. Model. Pract. Theory 34 (2013) 1–11.
[6] M. Doyle, T.F. Fuller, J. Newman, J. Electrochem. Soc. 140 (1993) 1526–1533.
[7] T.F. Fuller, M. Doyle, J. Newman, J. Electrochem. Soc. 141 (1994) 1–10.
[8] T.F. Fuller, M. Doyle, J. Newman, J. Electrochem. Soc. 141 (1994) 982–990.
[9] P. Arora, M. Doyle, A.S. Gozdz, R.E. White, J. Newman, J. Power Sources 88 (2000) 219–231.
[10] W. Luo, C. Lyu, L. Wang, L. Zhang, J. Power Sources 241 (2013) 295–310.
[11] J. Vazquez-Arenas, L.E. Gimenez, M. Fowler, T. Han, S.-k. Chen, Energy Convers. Manag. 87 (2014) 472–482.
[12] A. Tourani, P. White, P. Ivey, J. Power Sources 255 (2014) 360–367.
[13] L.H. Saw, Y. Ye, A.A.O. Tay, Energy Convers. Manag. 75 (2013) 162–174.
[14] K. Somasundaram, E. Birgersson, A.S. Mujumdar, J. Power Sources 203 (2012) 84–96.
[15] M. Doyle, J. Newman, A.S. Gozdz, C.N. Schmutz, J.M. Tarascon, J. Electrochem. Soc. 143 (1996) 1890–1903.
[16] E. Martinez-Rosas, R. Vasquez-Medrano, A. Flores-Tlacuahuac, Comput. Chem. Eng. 35 (2011) 1937–1948.
[17] M.G. Ouyang, G.M. Liu, L.G. Lu, J.Q. Li, X.B. Han, J. Power Sources 270 (2014) 221–237.
[18] X.B. Han, M.G. Ouyang, L.G. Lu, J.Q. Li, J. Power Sources 278 (2015) 802–813.
[19] S.K. Rahimian, S. Rayman, R.E. White, J. Power Sources 196 (2011) 8450–8462.
[20] B.S. Haran, B.N. Popov, R.E. White, J. Power Sources 75 (1998) 56–63.
[21] A. Romero-Becerril, L. Alvarez-Icaza, J. Power Sources 196 (2011) 10267–10279.
[22] S. Santhanagopalan, Q.Z. Guo, P. Ramadass, R.E. White, J. Power Sources 156 (2006) 620–628.
[23] M. Guo, G. Sikha, R.E. White, J. Electrochem. Soc. 158 (2011) A122–A132.
[24] A.P. schmidt, M. Bitzer, A.W. Imre, L. Guzzella, J. Power Sources 195 (2010) 5071–5080.
[25] W. Luo, C. Lyu, L. Wang, L. Zhang, Microelectron. Reliab. 53 (2013) 797–804.
[26] E. Tatsukawa, K. Tamura, Electrochim. Acta 115 (2014) 75–85.
[27] N. Baba, H. Yoshida, M. Nagaoka, C. Okuda, S. Kawauchi, J. Power Sources 252 (2014) 214–228.
[28] A.K. Sharma, C.Y. Ling, E. Birgersson, M. Vynnycky, M. Han, J. Power Sources 279 (2015) 345–350.
[29] M. Mastali Majdabadi, S. Farhad, M. Farkhondeh, R.A. Fraser, M. Fowler, J. Power Sources 275 (2015) 633–643.
[30] L. Cai, R.E. White, J. Electrochem. Soc. 156 (2009) A154–A161.
[31] L. Cai, R.E. White, J. Power Sources 217 (2012) 248–255.
[32] P.W.C. Northrop, V. Ramadesigan, S. De, V.R. Subramanian, J. Electrochem. Soc. 158 (2011) A1461–A1477.
[33] S. Khaleghi Rahimian, S. Rayman, R.E. White, J. Power Sources 224 (2013) 180–194.
[34] C. Ho, I.D. Raistrick, R.A. Huggins, J. Electrochem. Soc. 127 (1980) 343–350.
[35] H. Buschmann, S. Berendts, B. Mogwitz, J. Janek, J. Power Sources 206 (2012) 236–244.
[36] E. Deiss, Electrochim. Acta 47 (2002) 4027–4034.
[37] J.C. Forman, S.J. Moura, J.L. Stein, H.K. Fathy, J. Power Sources 210 (2012) 263–275.
[38] K. Thirugnanam, E.R.T.P. Joy, M. Singh, P. Kumar, Ieee Trans. Energy Convers. 29 (2014) 332–343.
[39] V.R. Subramanian, V.D. Diwakar, D. Tapriyal, J. Electrochem. Soc. 152 (2005) A2002–A2008.
[40] M. Guo, R.E. White, J. Power Sources 198 (2012) 322–328.
[41] C. Forgez, D.V. Do, G. Friedrich, M. Morcrette, C. Delacourt, J. Power Sources 195 (2010) 2961–2968.
[42] R.E. Gerver, J.P. Meyers, J. Electrochem. Soc. 158 (2011) A835–A843.
[43] Y.H. Ye, Y.X. Shi, A.A.O. Tay, J. Power Sources 217 (2012) 509–518.

Nomenclature

A_0:: effective heat dissipation area (m^2)
A:: effective area of electrodes (m^2)
c_0^l:: initial electrolyte concentration (mol m^{-3})
C_{can}:: heat capacity ratio of battery shell(J kg^{-1} K^{-1})
$c_{i,avg}^s$, $i = n, p$:: average Li-ion concentration in the active material in the electrodes (mol m^{-3})
$c_{i,surf}^s$, $i = n, p$:: surface Li-ion concentration in the active material in the electrodes (mol m^{-3})
$c_{i,0}^s$, $i = n, p$:: initial Li-ion concentration in the active material (mol m^{-3})
$c_{\max,i}^s$, $i = n, p$:: maximum Li-ion concentration in the active material (mol m^{-3})
C_p:: heat capacity ratio of wrapping body of electrode(J kg^{-1} K^{-1})
dE_{ocv}/dT_i, $i = n, p$:: entropy coefficients (V K^{-1})
$D_{s,i}$, $i = n, p$:: diffusion coefficient in the active material in the electrodes (m^2 s^{-1})
D_x:: maximum variation range of stoichiometric number x (−)
D_y:: maximum variation range of stoichiometric number y (−)
E_{ocv}:: open circuit voltage, OCV (V)
E_{ocv}^{ref}:: OCV at reference temperature (V)
F:: Faraday's constant (C mol^{-1})
G:: heat generation rate (W)
$G_{exchange}$:: heat dissipation rate (W)
h:: heat transfer coefficient (W m^{-2} K^{-1})
j_i, $i = n, p$:: pore wall flux of Li-ion on the intercalation particle of electrodes (mol m^{-2} s^{-1})
k_i, $i = n, p$:: reaction rate constant ($m^{2.5}$ $mol^{-0.5}$ s^{-1})
l_i, $i = n, p$:: thicknesses of electrodes (μm)
m_{can}:: mass of battery shell (kg)
m_{roll}:: mass of wrapping body of electrodes (kg)
P_{act}:: coefficient of anode reaction polarization ($m^{-1.5}$ $mol^{0.5}$ s)
P_{act}^{ref}:: coefficient of anode reaction polarization at reference temperature ($m^{-1.5}$ $mol^{0.5}$ s)
P_{con}:: proportional coefficient of liquid phase diffusion (mol m^{-3} A^{-1})
P_{con}^{ref}:: proportional coefficient of liquid phase diffusion at reference temperature (mol m^{-3} A^{-1})
Q_{all}:: total capacity at discharge rate of 0.02C (A s)
Q_i, $i = n, p$:: capacities of effective active material in the electrodes (A s)
Q_{ir}:: irreversible heat generation rate (W)
Q_r:: reversible heat generation rate (W)
$q_{i,avg}$, $i = n, p$:: volume-averaged concentration flux (mol m^{-4})
R:: ideal gas constant (J mol^{-1} K^{-1})
R_{amb}:: thermal resistance (K W^{-1})
R_{cond}:: thermal resistance (K W^{-1})
R_i, $i = n, p$:: particle radius (m)
R_{ohm}:: ohmic resistance (Ω)
R_{ohm}^{ref}:: ohmic resistance at reference temperature (Ω)
soc:: state of charge (−)
T:: battery internal temperature (K)
T_a:: ambient temperature (K)
T_{ref}:: reference temperature (K)
T_{surf}:: surface temperature (K)
t:: time (s)
t_+:: transport number (−)
U_i, $i = n, p$:: open circuit voltage curves (V)
x_0:: initial stoichiometric number of negative electrode (−)
x_{avg}:: solid phase average stoichiometric number of negative electrode (−)
x_{surf}:: solid phase surface stoichiometric number of negative electrode (−)
y_0:: initial stoichiometric number of positive electrode (−)
y_{avg}:: solid phase average stoichiometric number of positive electrode (−)
y_{surf}:: solid phase surface stoichiometric number of positive electrode (−)
y_{ofs}:: offset of relative position of stoichiometric numbers (−)
Δc^l:: electrolyte concentration deviation between two current collectors (mol m^{-3})
$\Delta x'$:: deviations between x_{surf} and x_{avg} (−)
$\Delta y'$:: deviations between y_{surf} and y_{avg} (−)
τ_i^s, $i = n, p$:: solid phase diffusion time constants of each electrode (s)
τ_e:: time constant of liquid phase diffusion (s)
ε_i:: porosity of the electrodes (−)
$\varepsilon_{f,n}$:: filler fraction of negative electrode (−)
$\varepsilon_{f,p}$:: filler fraction of positive electrode (−)
η_{act}:: reaction polarization overpotential (V)
η_{con}:: concentration polarization overpotential (V)
η_{ohm}:: ohmic polarization overpotential (V)
λ_{act}:: proportional coefficient of activation energy (K)

Subscript

λ_{con}:: proportional coefficient of activation energy (K)
λ_{ohm}:: proportional coefficient of activation energy (K)
act:: reaction
amb:: ambient
avg:: average
con:: concentration
max:: maximum
n:: negative
ohm:: ohmic
p:: positive
ref:: reference
surf:: surface